Proceedings of the 20th International Conference on Soil Mechanics and Geotechnical Engineering– Rahman and Jaksa (Eds)

Effect of rock joint spacing and joint stiffness on the stability of a cross-tunnel under seismic event using discrete element analysis

Effet de l'espacement des joints rocheux et de la rigidité des joints sur la stabilité d'un tunnel transversal sous un événement sismique à l'aide de l'analyse par éléments discrets

Kota Vijay Kiran & Ashish Juneja
Civil Engineering Department, IIT Bombay, India, kotavijaykiran@gmail.com

ABSTRACT: This study aims to assess the seismic response of a cross-tunnel intersection using a blocky system of distinct elements which follow the Lagrangian calculation scheme. A large model of two horse-shoe shaped cross tunnels was used. A discretized model was then generated using spacing and orientation of sets of joints acquired from scanline and surface mapping. The rock was modelled using Hoek Brown strength criteria, whilst the joints were modelled using the continuous yielding model to properly model the non-linear movement of the discontinuities. The analysis was done by varying the joints in frequency and space. And the other variables were the joint stiffnesses in the normal and shear direction. A non-uniform and localized displacement field was observed around the tunnel junction, which was dependent on the joint stiffnesses under static loading, and on the joint spacing in the case of seismic loading. Majority of the rock blocks near the tunnel periphery were detached under the dynamic event, with a marked reduction in its seismic resistance for high frequency jointed model with low joint stiffness compared to low joint frequency model with high stiffness. It was observed that the blocky rock mass has lesser self-arching capacity thereby has a potential of developing substantial dynamic response endangering integrity and stability of tunnel.

RÉSUMÉ : Cette étude tente d'évaluer la réponse sismique d'un tunnel croisé en utilisant un système en blocs d'éléments distincts qui suivent le schéma de calcul lagrangien. Un grand modèle de deux tunnels transversaux en forme de fer à cheval a été utilisé. Un modèle discrétisé a ensuite été généré en utilisant l'espacement et l'orientation des ensembles de joints acquis à partir de la cartographie de la ligne de balayage et de la surface. La roche a été modélisée à l'aide des critères de résistance de Hoek Brown, tandis que les joints ont été modélisés à l'aide du modèle de plastification continue pour modéliser correctement le mouvement non linéaire des discontinuités. L'analyse a été faite en faisant varier les articulations en fréquence et en espace. Et les autres variables étaient les rigidités articulaires dans la direction normale et de cisaillement. Un champ de déplacement non uniforme et localisé a été observé autour de la jonction tunnel, qui dépendait des raideurs des joints sous charge statique, et de l'espacement des joints en cas de charge sismique. La majorité des blocs de roche près de la périphérie du tunnel se sont détachés sous l'événement dynamique, avec une réduction marquée de sa résistance sismique pour le modèle articulé à haute fréquence avec une faible rigidité d'articulation par rapport au modèle à basse fréquence d'articulation avec une rigidité élevée. Il a été noté que le milieu discontinu possède une faible capacité d'auto-cambrage avec la possibilité de développer une réponse dynamique importante mettant en danger l'intégrité et la stabilité du tunnel.

KEYWORDS: Distinct element code, Earthquake loading, Rock joint stiffness, Tunnel intersection

1 INTRODUCTION.

Underground structures of complex interconnecting tunnels and shafts are increasingly being used for hydroelectric-power plants, nuclear waste repositories, ore-processing plants, warehouses and special military needs. Many earthquakes in the recent past have caused moderate to severe damage to underground facilities. For example, 1999 Du¨zce-Bolu (Bolu road tunnel, Turkey), 1999 Chi-Chi (Sanyi Railway tunnel, Taiwan), 1999 Kocaeli, 2004 Niigataken-Chuetsu (Uonuma and Wanazu tunnels, Japan), 2005 Kashmir (Muzaffarabad road tunnel) and 2008 Wenchuan (Longxi tunnel, China) earthquakes. The maximum damage was recorded in tunnels that are surrounded by discontinuities that are a guide for further devastation. Wang et al. (2001) reported the vulnerability of underground openings to earthquake loading considering the damaged state of numerous tunnels based on Taiwan's Chi-Chi earthquake.

Asakura et al. (2007), Yashiro et al. (2007) and Zhang (2013) investigated the earthquake-induced damage of the rock mountain tunnels. From the studies reported, it can be understood that, tunnel that pass through discontinuous media like jointed/ fractured rock are highly vulnerable to both static and dynamic loading conditions. Thus, the stability of these substantial underground structures against earthquake loading is of utmost importance.

Barton (1984) first considered the seismic load on underground structures using Q-value of rock mass classification system. Later, many researchers (Ahola, et al. 1996) reported the dynamic response of jointed rock tunnels based on the Lucky Friday Underground Mine of Coeur d'Alene Mining District of northern Idaho, USA. Aydan et al. 2010 carried out few experimental laboratory studies on breakable and non-breakable blocks using shake table tests to understand the behaviour of shallow unsupported tunnels. Numerical analyses on the shape, in-situ stress conditions and earthquake parameters (i.e. input wave direction and wave amplitude) was carried out by Genis (2002)), Genis & Aydan (2007) and Aydan & Genis (2014). Most of the research works reported considered modelling the tunnels in jointed rock using interface elements in the finite element approach which was based on continuum mechanics. However, its formulation is normally limited to minor displacements, and fails if many intersecting interfaces were used. Due to governing effects of the joints, it is not viable to assess the tunnel behaviour in jointed rock mass conditions via continuum-based analysis alone.

Thus, in order to overcome these limitations in finite element approach, the present study was carried by discrete element approach using 3DEC, focusing on the kinematics of blocky systems and the extent to which ground motions can trigger in the progressive slip of blocks adjacent to the excavation.

Tunnel-intersection of a cross tunnel, which is being investigated for developing underground research tunnel/s of Deep geological repositories in many countries has been adopted for the dynamic response analysis. In the present study, a horse-shoe shaped tunnel, forming an intersection due to access tunnel connecting to a larger tunnel has been adopted. To generate the rock joints Discrete Fracture Network (DFN) technique was attempted. The response of the tunnel intersection in jointed rock subjected to seismic excitation is studied here.

2 NUMERICAL MODEL EMPLOYING A DEM APPROACH

2.1 *Distinct Element Code (3DEC)*

In Discrete element method, rotation of discrete bodies as well as finite displacements are permitted. Along with complete detachment, automatic recognition of new joints are also allowed. The term 'Distinct Element Method (DEC)', proposed by Cundall (1971) represents Discrete element scheme having deformable contacts along with explicit transient schemes to solve equations of motion.

The material behavior in 3DEC was simulated using displacement and force interaction between distinct block elements. A step-by-step stress relaxation technique was implemented which alternated from Newton's laws of motion to stress-displacement function. Operating cycle here is found to depend upon the assumption that the blocks are either rigid or deformable as shown in Figure 1. Three main components were established in creating the rock mass model. The primary material component which occupies the volume was represented as an intact block of rock. Each block element was considered to obey the continuum mechanics and was simulated using finite difference method with constant strain tetrahedron grids. Discontinuities were incorporated in the continuum model using joint sets to represent the rock mass as a collection of blocks. As these discontinuities were treated as boundary conditions in this method, it was possible to permit block rotations and larger displacements along the discontinuities. The last component in the model generation is assigning the boundary conditions. The boundaries were assigned as velocity or stress boundaries to model the in-situ stresses and confinement. For estimating the force and displacement at the middle of the rigid block the following equations were used:

$$F_i = \sum F_i^c \tag{1}$$

$$\ddot{u} = \frac{F_i}{m} \tag{2}$$

Where, F_i^c is force at contact interface and m is mass of the block.

Unlike this, when it comes to deformable blocks, analysis has to be done for each zone element. Hourglass deformation error was eliminated by using the tetrahedron zone elements (Itasca, 2016). To determine the motion of every vertex of tetrahedron zone (grid point) a Gaussian surface of the following form was used.

$$\ddot{u} = g_i + \frac{\int \sigma_{ij} n_j ds + F_i}{m} \tag{3}$$

where s is the surface enclosing the lumped mass, m, at the grid point, F_i is resultant of all applied external forces at grid point, n_j is the unit normal to s, and g_i is the acceleration due to gravity.

The normal and tangential joint stiffness in between the blocks determine the mechanical calculations necessary at the contacts. Also, to calculate the relative displacements of the blocks (u_n and u_t) the interaction forces in the normal and tangential directions (F_n and F_t) along the contact points are made use. The contact surfaces either occur as vertex-to-edge contact or as edge-to-edge contact. In order to represent the contact surface slippage both linear and nonlinear relations including Coulomb slip (CS) model, Barton–Bandis (BB) model or Continuous Yielding (CY) joint models can be applied.

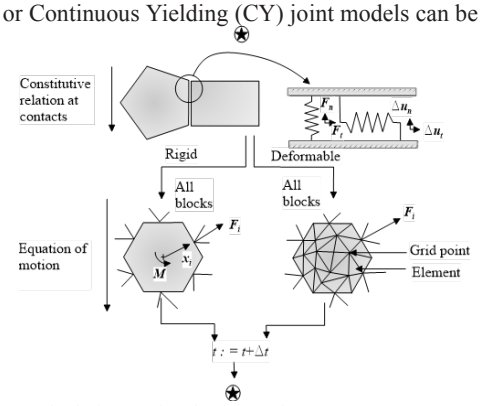

Figure 1. Calculation cycle of 3DEC (after Hart, 1993).

2.1 *Discrete Fracture Networks (DFN)*

Discrete Fracture Network (DFN) model is a numerical simulation of joints. In DFN module, fracture population can be imbibed into a rock mass model to represent a jointed/fractured rock mass. Several DFN formulations and computer codes have been developed in last two decades such as the FRACMAN, RESOBLOK and GEOFRAC. Recently, Itasca (2016) also incorporated the DFN module in 3DEC software version 5.0, upon the assumption that discrete fractures are disk-shaped. The DFN module in 3DEC presently supports the following geometrical characteristics: fracture size (or disk-diameters), densities (or intensities), orientation and position distributions. one of the important parameters in defining DFN is Fracture intensity, which can be given as an input based on the common measures used in practice like P_{10} (Number of fractures per unit length of a scanline), P_{21} (the total fracture length per unit area of a surface mapping) and P_{32} (Area of fractures per unit volume). The DFN modelling approach is controlled using its geometrical properties which follow an independent statistical distribution. From one (stochastic) DFN model, multiple DFN realizations can be created based upon the assumed random seed.

2.2 Choice of Joint Material Model

The behaviour of a jointed rock mass depends on the interface joint material model. For simulating joint deformability, linear Mohr-Coulomb (MC) friction model is considered the simplest model. MC model could be an appropriate choice for non-dilatant smooth discontinuities as in the case of faults at residual strength. In practice, it is more appropriate to define joints using non-linear material models such as continuously yielding model (CY) and Barton-Bandis (BB) model which replicate the actual behaviour rough rock joints. The Barton-Bandis (BB) model accounts for discontinuity strength and deformation behaviour considering the parameters like asperity roughness, joint roughness coefficient (JRC) and joint wall compressive strength (JCS). Nevertheless, the continuously yielding model introduced by Cundall & Hart (1984) provides more realistic behaviour of rock joints providing more coherent and unified discontinuity deformation of joints undergoing elastic deformations along with plastic deformations. The

model is adopted in the present study as by using a "bounding surface" concept it is capable of providing a continuous hysteretic damping for dynamic simulations.

2.2.1 Continuously Yielding Joint Model

Cundall and Hart (1984) introduced the continuously yielding joint model with the aim of simulating the internal mechanism of progressive damage of the joint asperities when under shear. Essential features of this model are listed below:

1. The curve of shear-stress versus shear-displacement always tends toward a "target" shear strength for the joint
2. The damage measure is accounted based on the target shear strength which decrease with increase in accumulated plastic displacement; and
3. The dilation angle is determined by taking the difference of apparent friction angle (determined by the current shear stress and normal stress) and residual friction angle (Itasca Consulting Group 2016).

For an applied normal loading, the joint response is defined in terms of joint normal stiffness and normal displacements as

$$\Delta\sigma_n = K_n \Delta u_n \tag{4}$$

where Δu_n is the normal displacement increment and K_n is the joint normal stiffness.
The joint normal stiffness can be represented as a function of the applied normal stress with two model parameters a_n and e_n.

$$K_n = a_n \sigma_n^{en} \tag{5}$$

In case of shear loading, the model shows a nonlinear behavior from the onset of shearing as presented in Figure 2. The change in shear-stress is expressed as

$$\Delta\tau = F K_s \Delta u_s \tag{6}$$

The shear stiffness, K_s, can be expressed in terms of the applied normal stress as

$$K_s = K_{si} \sigma_n^{es} \tag{7}$$

The shear stiffness in the equation (6) is governed by a factor F, which in turn depends upon the distance from the current stress curve to the bounding strength curve τ_m, (Figure 2) which is represented as

$$F = \frac{1 - \tau/\tau_m}{1 - r} \tag{8}$$

where τ is the current shear stress, τ_m is the failure stress at a given plastic displacement, and r is a factor which restores the elastic stiffness after load reversal. 'r' value initially set to zero. At the onset of a load reversal r is set to a value of τ/τ_m, thus F to 1. The bounding or target strength curve is described as

$$\tau_m = \sigma_n \tan(\phi_m) \tag{9}$$

where ϕ_m is the mobilized friction angle, which comprises both asperity sliding and shearing, ϕ_m can also be considered as the effective friction angle in case of no damage (i.e., no asperities shearing off). whereas, during shearing, when damage accumulate, the mobilized angle gets reduced based on the following equation

$$\Delta\phi_m = \frac{(\phi_m - \phi_b)}{R} \Delta u_s^p \tag{10}$$

where ϕ_b is the basic friction angle of rock joint interface, R is material parameter accounting for the joint roughness that defines ϕ_m and Δu_s^p is plastic displacement increment.
Δu_s^p can be expressed in terms of shear-displacement as

$$\Delta u_s^p = (1 - F)|\Delta u_s| \tag{11}$$

The incremental relation for ϕ_m, given by equation 10, is equivalent to

$$\phi_m = \phi_m^i - \phi_b) \exp(-u_s^p / R) + \phi_b \tag{12}$$

where ϕ_m^i is the initial friction angle which is the sum of basic friction angle and the initial asperity angle, $\phi_b + i_o$.
The effective dilatancy angle is then obtained from the basic friction angle along with the shear and normal stresses as

$$i = \tan(|\tau| / \sigma_n) - \phi_b \tag{13}$$

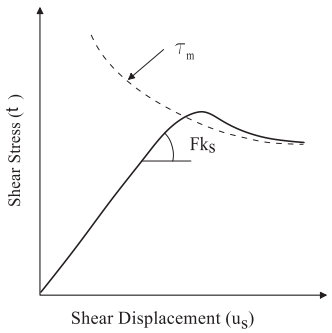

Figure 2. The CY joint model with bounding surface (Itasca, 2016)

3. MODELLING A CROSS-TUNNEL INTERSECTION IN JOINTED ROCK MEDIUM

3.1 *Model Setup*

A cross-tunnel intersection has been adopted with Horse-shoe shaped tunnel cross-section. The tunnel intersection comprises of an access tunnel (AT) which connects with an experimental chamber (EC). The access-tunnel is of dimension 6m x 6m x 3m. The experimental chamber is relatively larger than the access-tunnel with dimensions 15m x 15m x 3m. An assumption is made that tunnel is located at 120m deep from the top. The considered model dimensions for the analysis was 80mx80mx6m. The adopted model geometry ensures to have sufficient material around the tunnel and the boundaries shall not affect the outcome of the results. A discrete fracture network with joints set orientations as presented in Table 2 was established in the centre of the model of dimension 50mx80mx6m. Hoek-Brown constitutive model was employed for rock mass. The joints are modelled using the CY model as mentioned in previous sections. The input parameters of the rock mass and joint planes are presented in Table 2.

Table 1. Joint orientation summary

S. No.	Joint Dip (º)	Dip Direction (º)	Trace length (m)
1	50	270	12
2	80	10	9
3	70	150	10

For static analysis, initially the boundaries are fixed by assigning zero-velocity on all the four lateral sides and at the bottom of the model. At the top of the model corresponding to an overburden of 80m, vertical stress of 2.16 MPa was applied. For dynamic analysis, the top and bottom of the model are set as non-reflecting boundaries, and the seismic wave is applied at the base of the model as stress history during dynamic loading. A free-field dynamic boundary condition was adopted for seismic simulations, where in the four boundaries of the central mesh are connected to the free-field mesh by viscous dashpots as shown in Figure 4. This would simulate a quiet boundary condition. The free-field grid is solved in parallel with the central mesh. The free-field motions during the dynamic load are converted to traction, which are then transferred to the central mesh (main model). These two conditions of force transfer are given in Eqs. 14–16, which are transferred to the free-field mesh in the direction perpendicular to x-axis. The same would apply for the mesh boundaries on the other sides and corners (Itasca, 2016)

$$F_x = -\rho C_p (v_x^m - v_x^{ff})A + F_x^{ff} \quad (14)$$

$$F_x = -\rho C_s (v_y^m - v_y^{ff})A + F_y^{ff} \quad (15)$$

$$F_x = -\rho C_s (v_z^m - v_z^{ff})A + F_z^{ff} \quad (16)$$

where ρ is the density of the rock mass, C_p and C_s are the P-wave velocity and S-wave velocities, A is the influential area, v_i^m and v_i^{ff} are the velocities of a grid points in the central mesh, and in the free-field mesh respectively, acting in the i-th direction, and F_i^{ff} is the free-field grid point force in the i-direction. Rayleigh damping was also used for the rock medium considering a moderate value of 5 % for the analysis (Kuhlemeyer and Lysmer, 1973). As it is well known that the numerical accuracy of any dynamic analysis would depend on both frequency content and speed characteristics of the incident wave in a system, the element/zone size of the model is taken smaller than one-tenth to one-eighth of the wavelength of the input wave as described by Kuhlemeyer and Lysmer (1973). The element size considered as:

$$\Delta l \leq \left(\frac{1}{8} \approx \frac{1}{10}\right) L \quad (17)$$

Where L is the wavelength associated with the highest frequency component for peak velocities through the medium. In the case of discontinuum codes, this also applies to joint frequency (or block size). Hence, the maximum allowed element size calculated was 35 m. Hence to in the present study, to gain optimum performance, a central DFN zone was generated with a mesh size of 3 m and the top and bottom continuum blocks were generated with an mesh size of 5m.

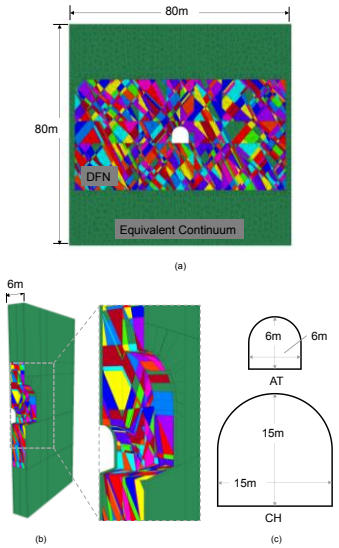

Figure 3. Representation of Tunnel model geometry and Free-field meshes

The model was established and applied gravitational stresses, solved until it reached equilibrium, checking the far field stresses for consistency. Then the excavation of tunnel is simulated. The dynamic runs were carried out after the excavation stage. A time domain dynamic analysis was performed by applying the 1989 Loma-Prieta earthquake dynamic record at the base of the model.

The acceleration-time history plot and corresponding Fourier amplitude spectra of the input ground motion are presented in Figures 5(a) and 5 (b) respectively.

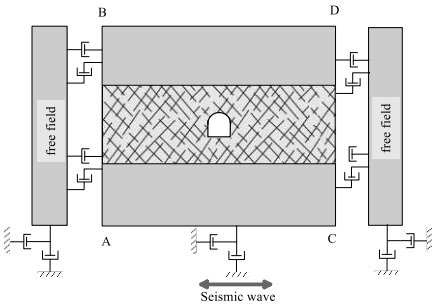

Figure 4. Scheme with the dynamic boundary conditions for seismic analysis with the representation of the free field blocks

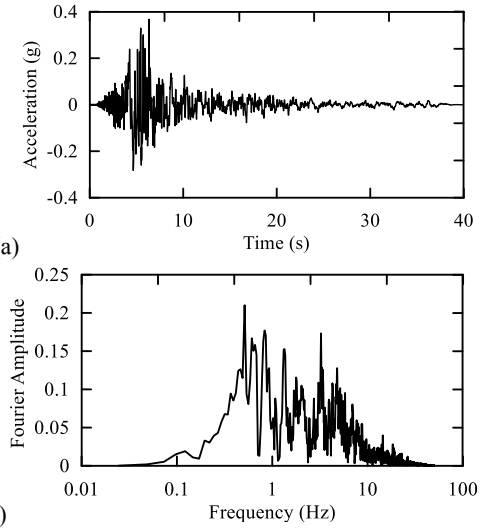

Figure 5. (a) Acceleration-time history of 1989 Loma-Prieta earthquake and its (b) Fourier amplitude spectra

4. RESULTS AND DISCUSSION

4.1 *Stress path*

The plastic zone contours after the earthquake loading are presented in Figures 6. The stress path of six monitoring points for the higher fracture intensity model with P_{32} = 2 m^2/m^3 were plotted in Figures (6(a-f)). The far field point is 'A' remains to be elastic throughout the earthquake period. The monitoring point 'B', located radially away from the tunnel shoulder, was elastic before applying the earthquake load. However, due to the application of dynamic load, the element experiences tensile stresses by the end of earthquake. Points C-F are located around the tunnel periphery and all the monitoring points were observed to be in tension due to the loss of confinement during excavation. The monitoring points ('C' and 'D') on the left spring line fails due to tension by the end of earthquake loading. This attributes to the unfavourable joint orientation, which drags the blocks formed into the opening. The monitoring points 'E' and 'F' located on the right side of the tunnel, fails in both tension and shear.

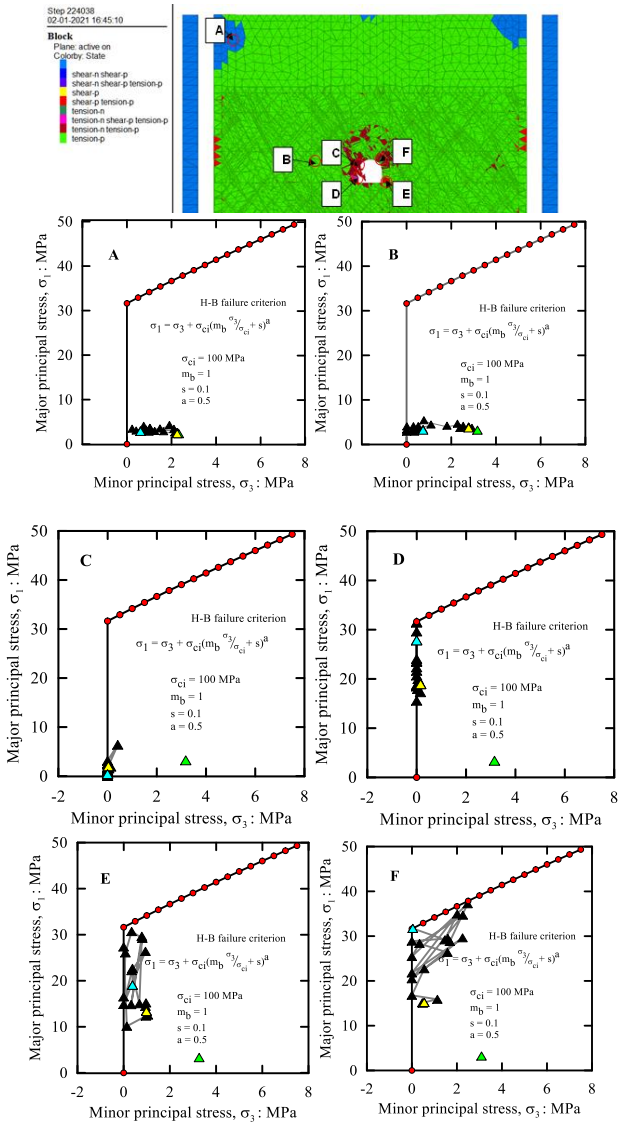

Figure 6. Stress path of the six monitoring points around the tunnel periphery

Table 2. Input parameters for of cross-tunnel model simulation.

	Parameter	Value/Type
Rock: Elastic Properties	Elastic type	Isotropic
	Young's Modulus (GPa)	45
	Poisson's Ratio	0.18
Strength Parameters	Failure Criterion	Generalized Hoek-Brown
	Material Type	Elastic
	Intact Comp. Strength (MPa)	100
	m_b -HB Parameter (peak)	1
	s – HB Parameter (peak)	0.001
	a – HB Parameter (peak)	0.5
Joint properties	Normal stiffness (a_n)	0.1-1000 GPa/m
	Shear stiffness (a_s)	0.1-1000 GPa/m
	Normal stiffness exponent (e_n)	0.0
	Shear stiffness exponent (e_s)	0.0
	Roughness parameter (R)	0.1 mm
	Intrinsic friction angle (ϕ_b)	30°
	Initial friction angle (ϕ^i_m)	59.3°

4.2 *Kinetic energy measurements*

The parametric study of the significance of joint stiffness on the tunnel response was conducted by analyzing the block velocities and their accumulated kinetic energy of the rock mass. For that purpose, initially, overall volume of individual blocks of the rock mass were identified, and subsequently their mass from the simulation. Furthermore, the grid points of the blocks were used to assess the velocity of individual blocks of the rock mass. Thus, the average kinetic energy was evaluated using the following expression

$$K_E = \frac{1}{2} m v_{av}^2 \qquad (18)$$

where K_E is kinetic energy of the blocks in kJ, m is mass in kg, and v_{av} is average velocity of the rock mass in m/s.

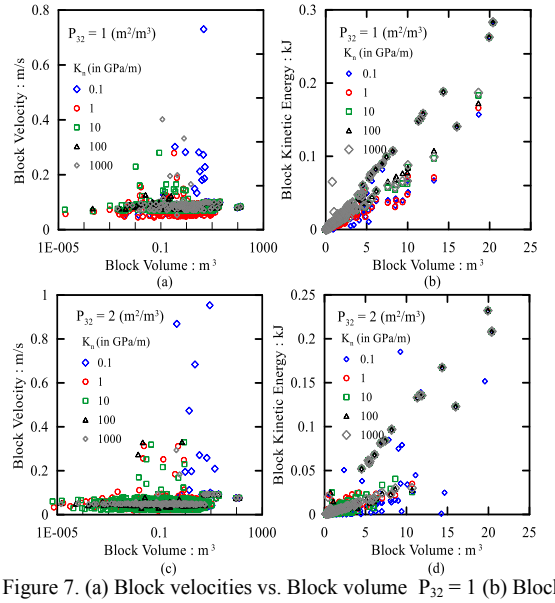

Figure 7. (a) Block velocities vs. Block volume P_{32} = 1 (b) Block Kinetic energy vs. Block volume P_{32} = 1 (c) Block velocities vs. Block volume P_{32} = 2

From analysing each individual blocks of the fractured rock mass, it was understood that the joint stiffness and joint network influences the block size as well as velocity. From

Figures 7 (a-d) it could be observed that, smaller blocks generally have higher (maximum) velocities, particularly in high fracture intensity models. On the contrary, huge blocks seems to have lower velocities but still higher kinetic energy due to their mass, and their contribution in total kinetic energy is also more. Based on preliminary observation, it was also noted that blocks close to excavation boundary was found to have more kinetic energy when compared to when it is placed deeper in rock mass. Figure 8 illustrates the significance of joint normal stiffness on the peak block velocity for the two fracture intensity models. In both the cases, the peal block velocity significantly reduces with an increase in joint normal stiffness from 0.1 to 1 GPa/m. whereas, the effect remains to be constant for joint stiffness above 1 GPa/m.

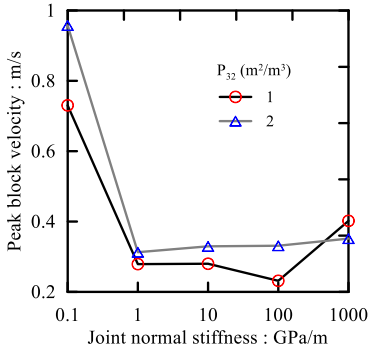

Figure 8. Peak block velocities vs. joint normal stiffness

4.3 *Plastic zones*

From Figure 9 the relationship between the plastic zone volume and the joint normal stiffness can be observed. Evidently, when joint stiffness exceeds 1, there is a significant reduction in the failure zone volume. However, in case of rock mass with P_{32}=2m^2/m^3, with higher number of joints, the plastic zone volume is very high, which impends to catastrophic failure of the tunnel.

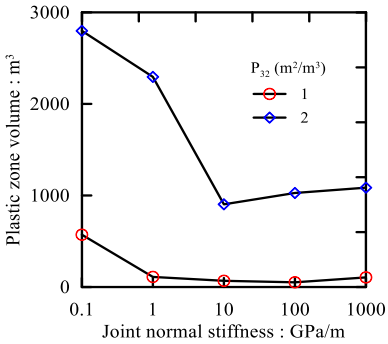

Figure 9. Plastic zone volume generated for varied joint normal stiffness

5 CONCLUSIONS

This paper aims to study the influence of joint spacing and stiffness on the seismic response of cross-tunnel intersection in jointed rock mass. The study takes advantage of using DEM, which can incorporate joints explicitly into the model and permits large displacements and rotation of blocks, for the investigation. The main findings of this study include:

- The stress path clearly depicts the tunnel tensile failure due to the applied dynamic load. The increase of zones in both tensile and shear when subjected to dynamic load was significant compared to the static condition.
- The role of joint orientation depicts the tunnel failure in either tension or shear. In the present study, tensile failure was predominant on the blocks situated on left sidewall of tunnel. However, blocks located on right sidewall of tunnel experience tension due to the loss of confinement during static load but fails in shear at the end of earthquake loading.
- The block velocities and kinetic energies measured implies that most of the rock blocks near the tunnel periphery were detached under the dynamic event, with a marked reduction in its seismic resistance for high frequency jointed model with low joint stiffness compared to low joint frequency model with high stiffness.
- It was observed that the blocky rock mass has lesser self-arching capacity thereby has a chance of developing substantial dynamic response endangering integrity and stability of tunnel.

6 ACKNOWLEDGEMENTS

The research was funded by the Board of Research in Nuclear Sciences (BRNS). First author would like to thank Nuclear Power Corporation of India Limited (NPCIL) for their necessary support.

7 REFERENCES

Aydan, O., Ohata, Y., Genis, M., Tokashiki, N., & Ohkubo, K. (2010). Response and stability of underground structures in rock mass during earthquakes. Rock Mechanics Rock Engg., 43, 857–875.

Ahola, M. P., Hsuing, S. M., & Kana, D. D. (1996). Experimental study on dynamic behavior of rock joints. Coupled thermo-hydro-mechanical process of fractured media. Developments in Geotechnical Engineering, 79, 467–506.

Asakura, T., Shiba, Y., Matsuoka, S., Oya, T., and Yashiro, K. (2007). Damage to mountain tunnels by earthquakes and its mechanism. Doboku Gakkai Ronbunshu, 659(659), 819–824.

Barton, N. (1984). Effects of rock mass deformation on tunnel performance in seismic regions. Advances in Tunnelling Technology and Subsurface Use, 4(3), 89–99.

Cundall, P.A. (1971). A computer model for simulating progressive large scale movements in blocky rock systems. In Proceedings of the symposium of the international society of rock mechanics, society for rock mechanics (ISRM), France (Vol. 1), P No. II-8.

Cundall, P.A., Hart, R.D., 1984. Analysis of Block Test No. 1 Inelastic Rock Mass Behavior: Phase 2 – A Characterization of Joint Behavior (Final Report). Itasca Consulting Group Report, Rockwell Hanford Operations, Subcontract SA-957.

Genis, M. & Aydan, Ö. (2007) Static and dynamic stability of a large underground opening. In: Proceedings of 2nd Symposium on Underground Excavations for Transportation. pp. 317–326.

Hart, R. D. (1993). An introduction to distinct element modelling for rock engineering. In Analysis and Design Methods (pp. 245–261). Pergamon Press, Oxford.

Itasca, 2016, 3DEC -Three-dimensional distinct element code. Ver. 5.2, User's Manual, Itasca Consulting Group, Minneapolis, USA.

Kuhlemeyer, R.L. and Lysmer. J. (1973) Finite Element Method Accuracy for Wave Propagation Problems. Journal of the Soil Dynamics Division, 99, 421-427.

Wang, W. L., Wang, T. T., Su, J. J., Lin, C. H., Seng, C. R., and Huang, T. H. (2001). Assessment of damage in mountain tunnels due to the Taiwan Chi-Chi Earthquake. Tunnelling Underground Space Technol. 16(3), 133–150.

Yashiro, K., Kojima, Y., and Shimizu, M. (2007). Historical earthquake damage to tunnels in Japan and case studies of railway tunnels in the 2004 Niigataken–Chuetsu earthquake. Quarterly Rep. Railway Tech. Res. Inst., 48(3), 136–141.